SCIENTIFIC REPORTS

OPEN

Analysis of the Conduction Mechanism and Copper Vacancy Density in p-type Cu_2O Thin Films

Received: 8 March 2017
Accepted: 5 June 2017
Published online: 18 July 2017

Sanggil Han & Andrew J. Flewitt

A quantitative and analytical investigation on the conduction mechanism in p-type cuprous oxide (Cu_2O) thin films is performed based on analysis of the relative dominance of trap-limited and grain-boundary-limited conduction. It is found that carrier transport in as-deposited Cu_2O is governed by grain-boundary-limited conduction (GLC), while after high-temperature annealing, GLC becomes insignificant and trap-limited conduction (TLC) dominates. This suggests that the very low Hall mobility of as-deposited Cu_2O is due to significant GLC, and the Hall mobility enhancement by high-temperature annealing is determined by TLC. Evaluation of the grain size and the energy barrier height at the grain boundary shows an increase in the grain size and a considerable decrease in the energy barrier height after high-temperature annealing, which is considered to be the cause of the significant reduction in the GLC effect. Additionally, the density of copper vacancies was extracted; this quantitatively shows that an increase in annealing temperature leads to a reduction in copper vacancies.

Cuprous oxide (Cu_2O) is a promising candidate as an active layer for p-type oxide semiconductor thin film transistors (TFTs). This is because hole-producing copper vacancies (V_{Cu}) are easily created due to their low formation energy, and effectively provide holes in Cu_2O because of the small acceptor ionisation energy (i.e. shallow acceptor level), which leads to intrinsically stable p-type conductivity[1]. Furthermore, comparable energy levels of Cu 3*d* and O 2*p* orbitals introduce considerable covalency into the ionic metal-oxide material system[1–3]. This not only reduces the localization of holes around negatively charged oxygen ions, but also disperses the valence band[1], which theoretically enables it to have a Hall mobility of ~270 $cm^2/V \cdot s$ at room temperature[4]. However, the presence of valence band tail states and potential barriers at grain boundaries leads to deposited thin films of Cu_2O having a significantly lower hole mobility compared with this theoretical limit.

To be specific, the nanocrystralline structure of thin Cu_2O films suggests the presence of potential energy barriers at grain boundaries. The effect of the potential barriers such as grain boundary scattering (i.e. grain-boundary-limited conduction, GLC) impedes hole transport[5,6]. Furthermore, if the width of the tail states in nanocrystalline materials is similar to or larger than the thermal energy at room temperature, the tail states also have a strong effect on carrier transport since a large number of thermally excited carriers are trapped at the band tail states[7]. Whilst the conduction band minimum (CBM) in Cu_2O is formed from spherical overlapping Cu 4*s* orbitals, the valence band maximum (VBM) is due to non-spherical Cu 3*d* orbitals which have spatial directivity, and thus they are sensitive to bonding angle disorder[8]. As in disordered silicon where the VBM is mainly composed of non-spherical *p* orbitals[9], this creates a broad distribution of localised tail states near the VBM of Cu_2O films. The Urbach energy (E_u) is a parameter reflecting the width of the tail states and thin Cu_2O films show an E_u larger than the thermal energy[8,10]. Thus, multiple carrier trapping and thermal release of holes in tail states (i.e. trap-limited conduction, TLC) also degrades transport in Cu_2O[11–13].

Post-deposition annealing of Cu_2O has been reported as one of the ways to enhance the performance of Cu_2O TFTs[14,15]. In a recent report[8], we showed that high-temperature annealing in vacuum leads to a significant improvement in the field-effect mobility and a reduction in the off-state current, mainly resulting from a film mobility (i.e. Hall mobility, μ_{Hall}) enhancement and a decrease in intrinsic carrier density (i.e. free hole concentration, p_{free}), respectively. The changes in μ_{Hall}, p_{free} and E_u according to annealing temperature (T_A) are summarized in Table 1.

In this paper, an analytical study on the conduction mechanism and the density of copper vacancies in Cu_2O thin films is presented in order to allow an in-depth discussion on the change in electrical characteristics of Cu_2O

Electrical Engineering Division, Department of Engineering, University of Cambridge, Cambridge, CB3 0FA, United Kingdom. Correspondence and requests for materials should be addressed to A.J.F. (email: ajf@eng.cam.ac.uk)

Annealing Temperature [°C]	As-deposited	500	600	700
μ_{Hall} [cm^2/V·s]	0.14	3.75	7.42	28
p_{free} [cm^{-3}]	1.68×10^{16}	1.30×10^{14}	7.34×10^{13}	1.85×10^{13}
E_u [meV]	223	166	128	78

Table 1. Summary of Parameters (μ_{Hall}, p_{free} and E_u) for Different Annealing Temperatures[8].

by high-temperature annealing. The effect of GLC on μ_{Hall} is quantified using a GLC coefficient (α_{GLC}) which is extracted from the difference between $p_{trap(Hall)}$ (the trapped hole concentration calculated from measured μ_{Hall} which includes the effects of TLC and GLC) and $p_{trap(DOS)}$ (the trapped hole concentration calculated based on extracted subgap density of states including only the TLC effect). Using the extracted α_{GLC} and Matthiessen's rule, the relative dominance of TLC and GLC is quantitatively assessed. The density of copper vacancies $\left(N_{V_{Cu}}\right)$ as a function of T_A was extracted using an equation derived from the charge neutrality condition, with consideration for ionized valence band tail states, and the formula for the ionized acceptor concentration. This work is important for an understanding of not only the dominant mobility degradation mechanism in Cu_2O but also the main cause of the mobility improvement by post-deposition annealing.

Results and Discussion

μ_{Hall} definition considering TLC and GLC. If carrier mobility is affected by several conduction mechanisms and they are independent of each other, Matthiessen's rule (i.e. $\mu^{-1} = \sum_i \mu_i^{-1}$, where μ_i denotes a mobility limited by a single conduction mechanism) can be applied. Using this rule, the effects of TLC and GLC can be incorporated into μ_{Hall} as follows,

$$\frac{1}{\mu_{Hall}} = \frac{1}{\mu_0} + \frac{1}{\mu_{TLC}} + \frac{1}{\mu_{GLC}} = \frac{1}{\mu_{0,TLC}} + \frac{1}{\mu_{GLC}}, \tag{1}$$

where μ_0, μ_{TLC} and μ_{GLC} are the free carrier mobility and the mobilities limited by TLC and GLC, respectively. Here, $\mu_0^{-1} + \mu_{TLC}^{-1}$ can be expressed as $\mu_{0,TLC}^{-1}$ (i.e. $\mu_0^{-1} + \mu_{TLC}^{-1} = \mu_{0,TLC}^{-1}$, where $\mu_{0,TLC}$ is the effective carrier mobility reduced by TLC). Using trap-limited conduction theory, $\mu_{0,TLC}$ can be defined by the product of μ_0 and β_{TLC} which is the ratio of free carrier concentration (p_{free}) to the total carrier concentration (i.e. $p_{free} + p_{trap}$) as follows[7],

$$\mu_{0,TLC} = \mu_0 \beta_{TLC}, \tag{2}$$

$$\beta_{TLC} = \left(\frac{p_{free}}{p_{free} + p_{trap}}\right), \tag{3}$$

where p_{trap} denotes the concentration of holes trapped in the valence band tail states. Using Equations (1) and (2), μ_{Hall} is then given by

$$\mu_{Hall} = \frac{\mu_0 \beta_{TLC} \mu_{GLC}}{\mu_0 \beta_{TLC} + \mu_{GLC}} = \mu_0 \alpha_{GLC} \beta_{TLC}, \tag{4}$$

$$\alpha_{GLC} = \frac{\mu_{GLC}}{\mu_0 \beta_{TLC} + \mu_{GLC}}. \tag{5}$$

Here, α_{GLC} is the GLC coefficient quantifying the effect of GLC on μ_{Hall} ($0 < \alpha_{GLC} \leq 1$, where $\alpha_{GLC} = 1$, i.e. $\mu_{GLC} \gg \mu_0 \beta_{TLC}$, represents the condition when μ_{Hall} is affected by only TLC).

Extraction of α_{GLC}. The GLC effect on μ_{Hall} was first quantified by extraction of α_{GLC}. The α_{GLC} can be determined based on the difference between $p_{trap(Hall)}$ and $p_{trap(DOS)}$. Specifically, using Equations (3) and (4), p_{trap} is given as follows,

$$p_{trap} = \left(\frac{\alpha_{GLC} \mu_0}{\mu_{Hall}} - 1\right) p_{free}. \tag{6}$$

Here, without considering α_{GLC}, i.e.

$$p_{trap(Hall)} = \left(\frac{\mu_0}{\mu_{Hall}} - 1\right) p_{free}, \tag{7}$$

$p_{trap(Hall)}$ can be obtained using measured μ_{Hall}, p_{free} and $\mu_0 = 270\,\text{cm}^2/\text{V}\cdot\text{s}$ (the theoretical limit of μ_{Hall} measured by longitudinal-optical (LO) phonon scattering at room temperature)[4,16]. If GLC affects hole transport, $p_{trap(Hall)}$ is overestimated since α_{GLC} ($0 < \alpha_{GLC} < 1$), and this reflects the degradation of μ_0 by GLC which is not considered

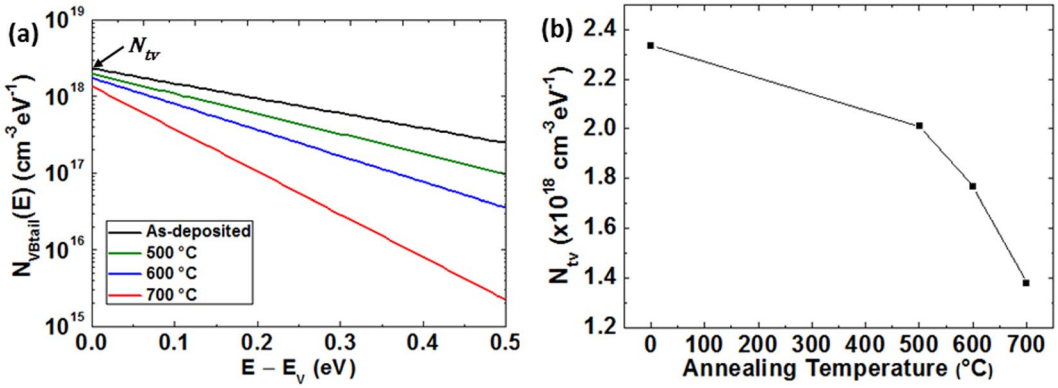

Figure 1. (**a**) Extracted density of tail states at the valence band ($N_{VBtail}(E)$) and (**b**) tail state density at $E = E_V$ (N_{tv}) of Cu_2O films before and after annealing.

in Equation (7). The α_{GLC} can be extracted from the overestimated extent of $p_{trap(Hall)}$ against $p_{trap(DOS)}$. The density of tail states at the valence band ($N_{VBtail}(E)$) can be approximated as an exponential distribution using O'Leary's model for the distribution of electronic states of disordered semiconductors as follows[17],

$$N_{VBtail}(E) = N_{tv}\exp\left(\frac{E_V - E}{E_u}\right), \tag{8}$$

$$N_{tv} = \frac{\sqrt{2}\,m_h^{*3/2}}{\pi^2\hbar^3}\sqrt{\frac{E_u}{2}}\exp\left(-\frac{1}{2}\right), \tag{9}$$

where E_V, N_{tv}, E_u, $\hbar$ and m_h^* are the valence band edge, the density of tail states at $E = E_V$, the Urbach energy reflecting the width of the tail states, the Planck constant and the density-of-states effective mass of holes in the valence band, respectively. Since valence band states of light holes are situated at the top of the valence band[18], the majority of holes are produced from the light hole band. For this reason, the band mass of light holes (m_{lh}) can be considered as m_h^*, which is about $0.56\,m_0$[18], where m_0 denotes the electron rest mass. Using Equations (8) and (9) and E_u in Table 1, $N_{VBtail}(E)$ and N_{tv} were extracted as seen in Fig. 1. The hole density trapped at the tail states ($p_{trap(DOS)}$) can be calculated using Equation (8) and the Fermi-Dirac distribution function (i.e. the probability of occupation of the donor-like tail states by an electron), $F(E) = 1/[1 + exp\{(E - E_F)/kT\}]$, where E_F is the Fermi energy, as

$$p_{trap(DOS)} = \int_{E_V}^{\infty} N_{VBtail}(E)[1 - F(E)]dE. \tag{10}$$

Here, we assumed that all ionised donor-like tail states filled with a hole (i.e. p_{trap}) are located above E_F (i.e. $F(E) = 0$ at $E > E_F$, $F(E) = 1$ at $E < E_F$), corresponding to the condition when the tail state energy $kT_t \cong E_u$ (T_t is the characteristic temperature of the tail states) is larger than the thermal energy kT (see Table 1)[11,19,20]. This yields the solution of Equation (10) as

$$p_{trap(DOS)} \approx N_{tv}E_u\exp\left(\frac{E_V - E_F}{E_u}\right). \tag{11}$$

In order to calculate $p_{trap(DOS)}$, $(E_V - E_F)$ was extracted from the measured p_{free} (see Table 1) and its formula given by the Boltzmann approximation[21],

$$p_{free} = N_V\exp\left(\frac{E_V - E_F}{kT}\right). \tag{12}$$

N_V is the effective density of states for free carriers in the valence band and is calculated using[21]

$$N_V \equiv 2\left(\frac{2\pi m_h^* kT}{\hbar^2}\right)^{3/2}. \tag{13}$$

For $m_h^* = 0.56\ m_0$, N_V was calculated to be $1.05 \times 10^{19}\,cm^{-3}$. Using the calculated N_V and Equation (12), we obtained $E_V - E_F = -0.166$ eV (as-deposited), -0.29 eV (500 °C), -0.31 eV (600 °C) and -0.34 eV (700 °C). $p_{trap(DOS)}$ was estimated using these parameters, extracted N_{tv} (see Fig. 1b), E_u in Table 1 and Equation (11), and $p_{trap(Hall)}$ was calculated using Equation (7) as seen in Fig. 2a. In order to check the extent of the discrepancy between $p_{trap(Hall)}$ and $p_{trap(DOS)}$, we assumed $\alpha_{GLC} = 1$ for $T_A = 700$ °C (i.e. $p_{trap(Hall)}$ (700 °C) = p_{trap} (700 °C)) based on the fact that a Cu_2O TFT annealed at 700 °C follows the Meyer-Neldel (MN) rule indicating that carrier transport is

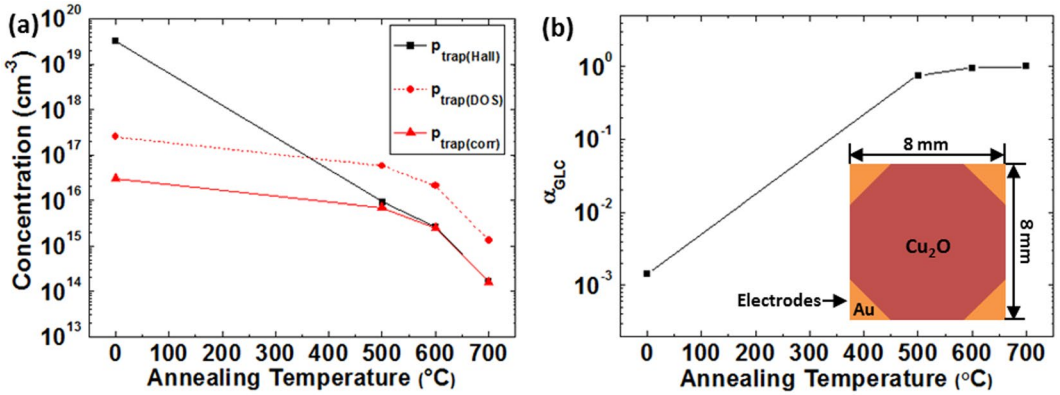

Figure 2. (**a**) $p_{trap(Hall)}$, $p_{trap(DOS)}$ and $p_{trap(corr)}$ and (**b**) α_{GLC} as a function of annealing temperature. Inset shows the schematic van der pauw geometry for the Hall measurement. (**a**) shows the discrepancy between $p_{trap(Hall)}$ (calculated using μ_{Hall} including the effects of TLC and GLC) and $p_{trap(corr)}$ (i.e. $p_{trap(DOS)}$ corrected using $p_{trap(Hall)}$ (700 °C)) including only the TLC effect. In (**b**), the effect of GLC on μ_{Hall} is quantified by α_{GLC} (extracted using Equation (15) and the difference between $p_{trap(Hall)}$ and $p_{trap(corr)}$). This shows that α_{GLC} approaches unity as annealing temperature increases: 0.0014 (as-deposited), 0.76 (500 °C), 0.96 (600 °C), 1 (700 °C). This suggests that GLC becomes insignificant after high-temperature annealing.

governed by trap-limited conduction[13,22] (see Supplementary Fig. S1), and $p_{trap(DOS)}$ was corrected by the product of $p_{trap(DOS)}$ (normalized to the value at $T_A = 700$ °C) and $p_{trap(Hall)}$ (700 °C) (see $p_{trap(corr)}$ in Fig. 2a). Note that $p_{trap(Hall)}$ values for all cases except the material annealed at 700 °C (i.e. $\alpha_{GLC} < 1$) are overestimated p_{trap} values which are simply used for the extraction of α_{GLC}; they are not actual values of p_{trap}. Figure 2a shows a large discrepancy between $p_{trap(Hall)}$ and $p_{trap(corr)}$ for the as-deposited film; the discrepancy decreases significantly after high-temperature annealing. Representing Equation (6) allowing for α_{GLC} and explicitly including $p_{trap(Hall)}$ and $p_{trap(corr)}$ gives

$$p_{trap(corr)} = \left[\left(\frac{\mu_0}{\mu_{Hall}} - 1\right) - \frac{\mu_0}{\mu_{Hall}}(1 - \alpha_{GLC})\right]p_{free} = p_{trap(Hall)} - \frac{p_{free}\mu_0}{\mu_{Hall}}(1 - \alpha_{GLC}). \tag{14}$$

α_{GLC} is then given by

$$\alpha_{GLC} = 1 - \frac{\mu_{Hall}}{\mu_0}\left(\frac{p_{trap(Hall)} - p_{trap(corr)}}{p_{free}}\right). \tag{15}$$

Using Equation (15) and the difference between $p_{trap(Hall)}$ and $p_{trap(corr)}$, α_{GLC} values as a function of T_A were finally extracted as shown in Fig. 2b. This shows that a very low α_{GLC} (~0.001) of the as-deposited film increases significantly after annealing at 500 °C and α_{GLC} approaches unity as T_A increases further. This suggests that GLC significantly affects hole transport in as-deposited Cu_2O but the effect of GLC on hole transport becomes insignificant after high-temperature annealing.

Extraction of $\mu_{0,GLC}$ and μ_{TLC} from μ_{Hall}. $\mu_{0,GLC}$ (the effective carrier mobility reduced by GLC) and μ_{TLC} were extracted from the measured μ_{Hall} using the extracted α_{GLC} and Matthiessen's rule in order to quantitatively investigate the relative dominance of TLC and GLC. μ_{GLC} is given using Equation (5) and $\mu_{Hall} = \mu_0\alpha_{GLC}\beta_{TLC}$ (see Equation (4)) as follows,

$$\mu_{GLC} = \frac{\mu_0\alpha_{GLC}\beta_{TLC}}{1 - \alpha_{GLC}} = \frac{\mu_{Hall}}{1 - \alpha_{GLC}}. \tag{16}$$

The assumption ($\alpha_{GLC} = 1$ for $T_A = 700$ °C, i.e. GLC has no effect on carrier mobility) leads to $\mu_{GLC} = \infty$, which physically means the relative insignificance of GLC compared to TLC (i.e. $\mu_{GLC} \gg \mu_{TLC}$), not actually infinite μ_{GLC}. Because of the calculated infinite value of μ_{GLC} for $T_A = 700$ °C, $\mu_{0,GLC}$ was calculated using Matthiessen's rule (i.e. $\mu_{0,GLC}^{-1} = \mu_0^{-1} + \mu_{GLC}^{-1}$) and Equation (16) for a quantitative comparison with μ_{TLC},

$$\mu_{0,GLC} = \frac{\mu_0\mu_{Hall}}{\mu_0(1 - \alpha_{GLC}) + \mu_{Hall}}. \tag{17}$$

μ_{TLC} was calculated using the following equation derived from Matthiessen's rule (i.e. $\mu_{Hall}^{-1} = \mu_0^{-1} + \mu_{GLC}^{-1} + \mu_{TLC}^{-1} = \mu_{0,GLC}^{-1} + \mu_{TLC}^{-1}$),

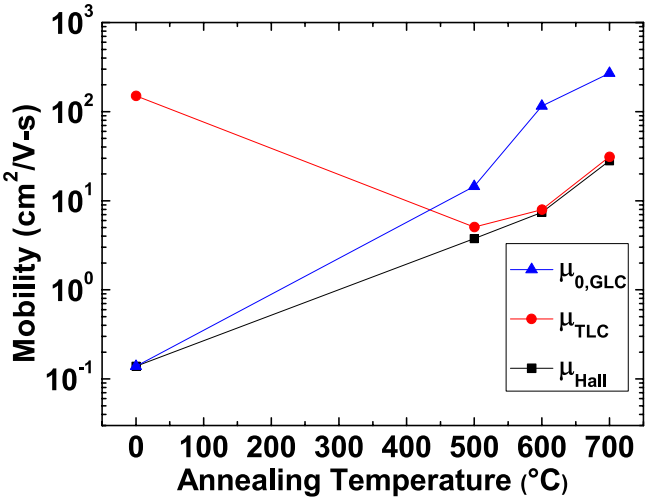

Figure 3. Measured μ_{Hall}, extracted μ_{TLC} and $\mu_{0,GLC}$ as a function of annealing temperature. μ_{Hall} is entirely determined by $\mu_{0,GLC}$ for the as-deposited Cu_2O thin film, whereas μ_{Hall} is limited by μ_{TLC} after high-temperature annealing, which suggests that GLC dominates before annealing and TLC becomes dominant after high-temperature annealing.

$$\mu_{TLC} = \frac{\mu_{0,GLC}\mu_{Hall}}{\mu_{0,GLC} - \mu_{Hall}}. \tag{18}$$

The calculated results (see Fig. 3) show that μ_{Hall} of as-deposited Cu_2O is governed by GLC, suggesting that the very low μ_{Hall} of the Cu_2O thin film before annealing is due to the considerable GLC. In contrast, GLC becomes insignificant and therefore TLC dominates after post-deposition annealing at temperatures $\geq$500 °C.

Explanation for the change in the effects of GLC & TLC. To explain the reduction in the GLC effect with an increase in T_A, changes in the grain size (L) and the energy barrier height at the grain boundary (E_B) were examined. SEM images (see Fig. 4a) show that L tends to increase with increasing T_A, but it is hard to quantitatively provide L values since annealed thin films have irregular grains. In order to examine the change in L quantitatively, L was extracted from the Scherrer equation[23] (i.e. $L = 0.94\lambda/(\beta\cos\theta)$) using the line broadening of the intense Cu_2O (200) peak of the XRD patterns reported in the authors' previous paper[8]. Here, λ and θ are the X-ray wavelength of Cu $K_{\alpha 1}$ radiation (0.154 nm) and the Bragg angle, respectively, and β denotes the full width at half maximum (FWHM) corrected by $(\beta_m^2 - \beta_i^2)^{1/2}$ where β_m and β_i are the measured and instrumental FWHM in radians. The grain sizes from the SEM images (see Fig. 4a) and extracted from the Scherrer equation (see Fig. 4b) do not match exactly. This can be understood by considering that the grain size observed from the SEM images can be different from the extracted value since the SEM images show a small surface area while XRD samples the area of the X-ray beam size (the beam diameter: ~500 μm). The effective mobility by GLC is given as $\mu_{0,GLC} = Lq\sqrt{1/2\pi m^* kT}\exp(-E_B/kT)$, where q is the elementary charge[5]. Using this equation, the E_B is expressed as

$$E_B = -kT\ln\left(\frac{\mu_{0,GLC}\sqrt{2\pi m^* kT}}{Lq}\right). \tag{19}$$

E_B was calculated using the extracted values (i.e. L and $\mu_{0,GLC}$) and Equation (19). The calculated results (see Fig. 4b) quantitatively show that an increase in T_A leads to an increase in L and a decrease in E_B, which provides a clear explanation for the reduction in the GLC effect. Additionally, E_B decreases to $E_B < kT$ (i.e. ~26 meV at 300 K) at T_A = 700 °C, which is considered to be the main reason for the insignificance of GLC in the 700 °C-annealed Cu_2O thin film. In addition, based on Equations (2) and (3), the change in μ_{TLC} can be explained by the variation in β_{TLC} (i.e. the ratio of p_{free} to $p_{free} + p_{trap}$). Figure 4c shows calculated p_{free}, $p_{trap} = p_{trap(corr)}$, $p_{total} = p_{free} + p_{trap}$ and β_{TLC} when E_u = 223 meV (extracted from the as-deposited case) as a function of $E_F - E_V$. This clearly shows that μ_{TLC} is affected by not only E_u but also the position of E_F. Specifically, as $E_F - E_V$ decreases, p_{free} increases more significantly than p_{trap} due to $(kT)^{-1} > (E_u)^{-1}$ and therefore β_{TLC} approaches unity as seen in Fig. 4c. This means a reduction in the TLC effect as E_F approaches to E_V. Figure 4d shows the calculated β_{TLC} of all the samples (i.e. when E_u = 223 meV (as-deposited), E_u = 166 meV (500 °C), E_u = 128 meV (600 °C) and E_u = 78 meV (700 °C)) as a function of $E_F - E_V$. If all the samples had the same E_F, the as-deposited film with the highest E_u would lead to the lowest β_{TLC}. However, since $E_F - E_V$ of the as-deposited film is much smaller compared to annealed films, its β_{TLC} is the highest, as seen in Fig. 4d, which is the reason for the relatively insignificant TLC effect in the as-deposited film.

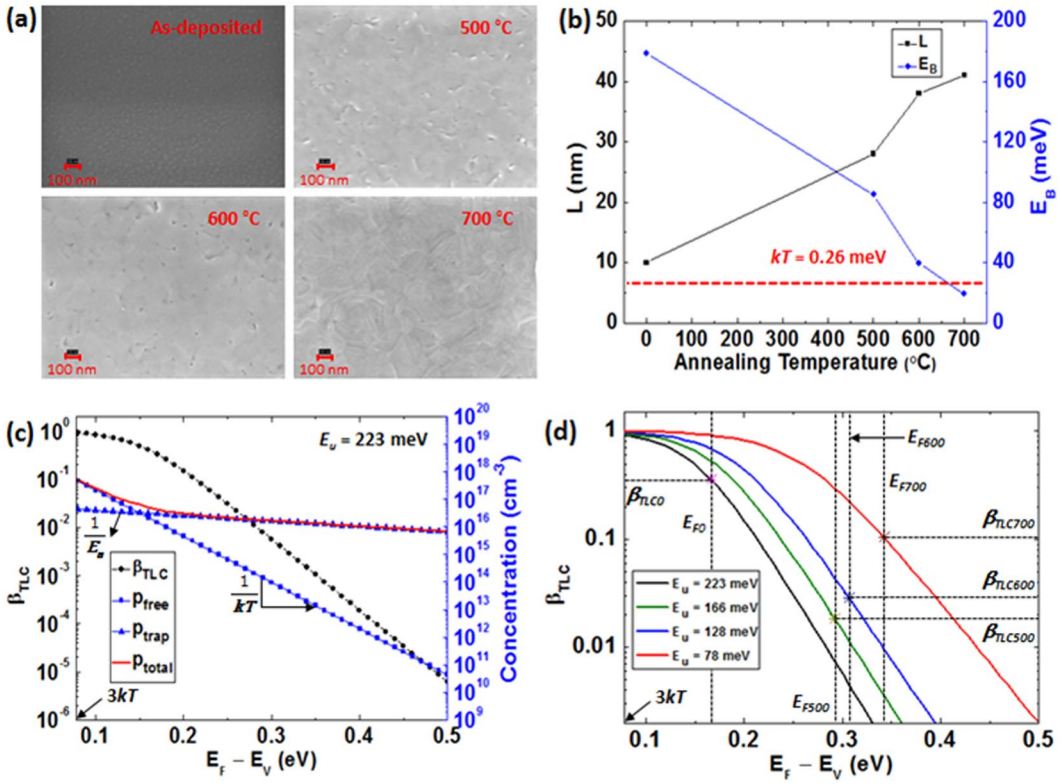

Figure 4. (**a**) SEM images of the surface of as-deposited and annealed Cu_2O films, (**b**) the estimated grain size (L) and energy barrier height at grain boundaries (E_B) as a function of annealing temperature, (**c**) calculated p_{free}, p_{trap}, p_{total} and β_{TLC} when $E_u = 223$ meV and (d) β_{TLC} when $E_u = 223$ meV (as-deposited), $E_u = 166$ meV (500 °C), $E_u = 128$ meV (600 °C) and $E_u = 78$ meV (700 °C) as a function of $E_F - E_V$. In (**b**), the red dot line shows the thermal energy at room temperature. In (**c**), p_{free} was calculated using Equation (12) given by Boltzmann's approximation which is valid for $E_F - E_V \geq 3\,kT$. In (**d**), E_{F0}, E_{F500}, E_{F600} and E_{F700} denote the Fermi energy of the as-deposited film and 500, 600 and 700 °C-annealed films, and the corresponding β_{TLC} values are $\beta_{TLC0} = 0.36$, $\beta_{TLC500} = 0.018$, $\beta_{TLC600} = 0.029$ and $\beta_{TLC700} = 0.1$, respectively.

The density of copper vacancies $\left(N_{V_{Cu}}\right)$. As seen in Table 1 and Fig. 2a, an increase in T_A leads to a reduction in the total hole concentration ($p_{free} + p_{trap}$), suggesting a decrease in V_{Cu} which is the main hole producer in Cu_2O. In order to provide a quantitative insight into the reduction in V_{Cu} with an increase in T_A, the density of copper vacancies, $N_{V_{Cu}}$, was extracted using the following method. This method begins with the charge neutrality condition, $p + N_D^+ = n + N_A^-$, where p, n, N_D^+ and N_A^- are the densities of free holes, free electrons, ionized donors and ionized acceptors, respectively. Since Cu_2O films have valence band tail states (i.e. donor-like states) and holes are trapped at the tail states, the density of ionized tail states (N_{TS}^+) should be added into the charge neutrality condition (i.e. $p + N_D^+ + N_{TS}^+ = n + N_A^-$). This becomes $p + N_{TS}^+ \approx N_A^-$ by considering N_D^+ and n to be negligible (i.e. $p + N_{TS}^+ \gg N_D^+, N_A^- \gg n$). In addition, since another possible hole producer (the oxygen interstitial, O_i) has deep acceptor levels, it can be assumed that V_{Cu} with the shallow acceptor level dominates the generation of holes in Cu_2O[1]. Thus, N_A^- can be substituted with the density of ionized V_{Cu} $\left(N_{V_{Cu}}^-\right)$. Finally, because $N_{TS}^+ = p_{trap}$, we can obtain the following equation,

$$N_{V_{Cu}}^- \approx p_{free} + p_{trap}. \tag{20}$$

Using the formula describing the fraction of ionized acceptor concentration[21], $N_{V_{Cu}}^-$ could be given as follows,

$$N_{V_{Cu}}^- = \frac{N_{V_{Cu}}}{1 + g_A \exp\left(\frac{E_{V_{Cu}} - E_F}{kT}\right)}, \tag{21}$$

where g_A and $E_{V_{Cu}}$ are the acceptor-site degeneracy factor and the energy level of copper vacancies, respectively. Here, representing $E_{V_{Cu}} - E_F$ as $(E_{V_{Cu}} - E_V) + (E_V - E_F)$, Equation (21) can be expressed as

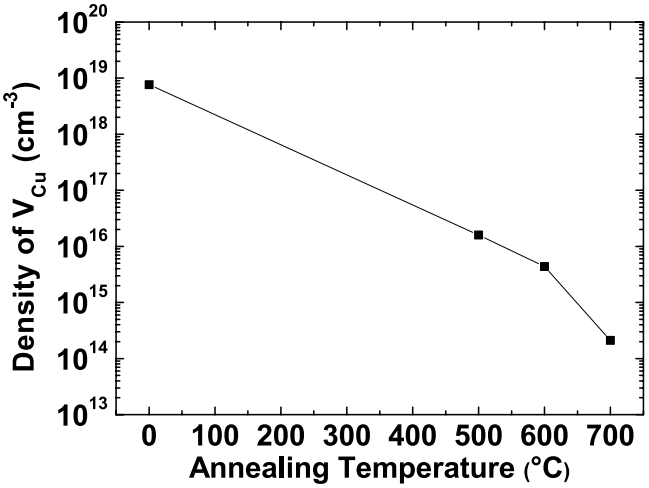

Figure 5. Extracted density of copper vacancies as a function of annealing temperature.

$$N_{V_{Cu}}^{-} = \frac{N_{V_{Cu}}}{1 + g_A \exp\left(\frac{E_{V_{Cu}} - E_V}{kT}\right)\exp\left(\frac{E_V - E_F}{kT}\right)}, \tag{22}$$

Using Equations (12), (20) and (22), $N_{V_{Cu}}$ is expressed as

$$N_{V_{Cu}} = (p_{free} + p_{trap})\left[1 + g_A \exp\left(\frac{E_{V_{Cu}} - E_V}{kT}\right)\frac{p_{free}}{N_V}\right]. \tag{23}$$

Here, $E_{V_{Cu}} - E_V = 0.28$ eV is used; this has been calculated by density-functional theory (DFT)[1]. Since Cu_2O has one degenerate valence band (Γ_7^+) at the VBM[18], each copper vacancy state (i.e. each acceptor state) can accept one hole with either spin or have no hole[21], and hence $g_A = 2$. Using these parameters (i.e. the measured p_{free}, calculated $p_{trap(corr)}$ for p_{trap} and Equation (23)), $N_{V_{Cu}}$ was extracted as seen in Fig. 5, which quantitatively shows a significant decrease in V_{Cu} with an increase in T_A.

Conclusions

In conclusion, this paper shows that grain-boundary-limited conduction becomes insignificant and carrier transport is governed by trap-limited conduction after high-temperature annealing. This is explained by a considerable reduction in the energy barrier height at the grain boundaries and an increase in the grain size by high-temperature annealing, suggesting that the GLC effect on hole transport in Cu_2O can be reduced significantly by post-deposition annealing. In addition, an increase in annealing temperature gives rise to a decrease in the total hole concentration, suggesting a reduction in copper vacancies, which is the main origin of holes in Cu_2O. An extraction method for the density of copper vacancies $\left(N_{V_{Cu}}\right)$ is proposed and the consequent calculation of $N_{V_{Cu}}$ quantitatively shows a significant decrease in copper vacancy density with annealing.

Methods

Film Fabrication. Deposition of Cu_2O was performed by remote-plasma reactive sputtering using a high target utilization sputtering (HiTUS) system (Plasma Quest Limited) without intentional substrate heating (see a schematic diagram of HiTUS[24]). The chamber was pumped to a base pressure of 6.0×10^{-6} mbar and Ar gas was supplied to set a process pressure of 1.5×10^{-3} mbar. Ar plasma was generated by an RF launch power of 1.2 kW in a remote chamber and then directed onto a metallic copper target with 4 inch diameter and 99.999% purity by electromagnets in the chamber. The reactive sputtering was performed at an oxygen flow rate of 16 sccm and a DC bias power of 0.95 kW with a DC bias voltage of ~690 V.

Cu_2O samples with film thickness of ~500 nm were deposited on quartz (Spectrosil B) and 8 mm × 8 mm glass (Corning 7059) substrates. The thickness was determined using surface profilometry (Veeco Dektak 200SI). The as-deposited Cu_2O was subsequently annealed in vacuum (9.5×10^{-4} mbar) in an Aixtron Cambridge Nanoinstruments Black Magic 2 system at various temperatures (500, 600 and 700 °C) for 10 min. The temperature ramp rate, cooling time and unloading temperature were 5 °C/s, 20 min and 50 °C, respectively. Annealing temperature was monitored with an infrared (IR) radiation pyrometer (Infratherm IGA8 plus). In order to perform Hall measurements using the van der Pauw method, four Au electrodes were thermally evaporated at the corners of the Cu_2O film deposited on 8 mm × 8 mm glass substrates through a shadow mask.

Measurement. In order to obtain electrical characteristics (i.e. Hall mobility and carrier density) of Cu_2O films, Hall measurements at room temperature were carried out using an MMR Technologies Hall Effect Measurement System (K2500-7). For extraction of the Urbach energy (E_u), the optical absorption coefficient

($\alpha(\upsilon)$) was obtained using an ATI Unicam UV/Vis spectrometer (UV2-200) and Cu_2O films formed on quartz substrates. Based on the relation between $\alpha(\upsilon)$ and E_u, $\alpha(\upsilon) = \alpha_0 \exp(h\upsilon/E_u)$, E_u was extracted from the reciprocal of the slopes of the linear region of an $\ln(\alpha)$ versus $h\upsilon$ plot[8].

Data Availability. The datasets generated during and/or analysed during the current study are available in the Cambridge University Data Repository (http://www.repository.cam.ac.uk/).

References

1. Raebiger, H., Lany, S. & Zunger, A. Origins of the p-type nature and cation deficiency in Cu_2O and related materials. *Phys. Rev. B* **76**, 045209 (2007).
2. Kawazoe, H., Yanagi, H., Ueda, K. & Hosono, H. Transparent p-type conducting oxides: design and fabrication of p-n heterojunctions. *MRS Bull.* **25**, 28–36 (2000).
3. Yanagi, H., Kawazoe, H., Kudo, A., Yasukawa, M. & Hosono, H. Chemical design and thin film preparation of p-type conductive transparent oxides. *J. Electroceram.* **4**, 407–414 (2000).
4. Lee, Y., Winkler, M. T., Siah, S. C., Brandt, R. & Buonassisi, T. Hall mobility of cuprous oxide thin films deposited by reactive direct-current magnetron sputtering. *Appl. Phys. Lett.* **98**, 192115 (2011).
5. Seto, J. Y. W. The electrical properties of polycrystalline silicon films. *J. Appl. Phys.* **46**, 5247–5254 (1975).
6. Nam, D. *et al*. Active layer thickness effects on the structural and electrical properties of p-type Cu_2O thin-film transistors. *J. Vac. Sci. Technol. B* **30**, 060605 (2012).
7. Konenkamp, R. *Photoelectric Properties and Applications of Low-Mobility Semiconductors* Chap. 2 (Springer, 2000).
8. Han, S., Niang, K. M., Rughoobur, G. & Flewitt, A. J. Effects of post-deposition vacuum annealing on film characteristics of p-type Cu_2O and its impact on thin film transistor characteristics. *Appl. Phys. Lett.* **109**, 173502 (2016).
9. Robertson, J. & Falabretti, B. *Handbook of Transparent Conductors* (ed. Ginley, D. S.) Chap. 2 (Springer, 2011).
10. Wang, Y. *et al*. Transmittance enhancement and optical band gap widening of Cu_2O thin films after air annealing. *J. Appl. Phys.* **115**, 073505 (2014).
11. Street, R. A. *Hydrogenated Amorphous Silicon* (Cambridge University Press, 2005).
12. Lee, S. & Nathan, A. Localized tail state distribution in amorphous oxide transistors deduced from low temperature measurements. *Appl. Phys. Lett.* **101**, 113502 (2012).
13. Jeong, C. *et al*. Investigation of the charge transport mechanism and subgap density of states in p-type Cu_2O thin-film transistors. *Appl. Phys. Lett.* **102**, 082103 (2013).
14. Fortunato, E. *et al*. Thin-film transistors based on p-type Cu_2O thin films produced at room temperature. *Appl. Phys. Lett.* **96**, 192102 (2010).
15. Sohn, J. *et al*. Effects of vacuum annealing on the optical and electrical properties of p-type copper-oxide thin-film transistors. *Semicond. Sci. Technol.* **28**, 015005 (2013).
16. Shimada, H. & Masumi, T. Hall mobility of positive holes in Cu_2O. *J. Phys. Soc. Jpn.* **58**, 1717–1724 (1989).
17. O'Leary, S. K., Johnson, S. R. & Lim, P. K. The relationship between the distribution of electronic states and the optical absorption spectrum of an amorphous semiconductor: An empirical analysis. *J. Appl. Phys.* **82**, 3334–3340 (1997).
18. Meyer, B. K. *et al*. *Oxide Semiconductors* (ed. Svensson, B. G.) Chap. 6 (Elsevier, 2013).
19. Lee, S., Ahnood, A., Sambandan, S., Madan, A. & Nathan, A. Analytical field-effect method for extraction of subgap states in thin-film transistors. *IEEE Elec. Devi. Lett.* **33**, 1006–1008 (2012).
20. Lee, S., Nathan, A., Ye, Y., Guo, Y. & Robertson, J. Localized tail states and electron mobility in amorphous ZnON thin film transistors. *Sci. Rep.* **5**, 13467 (2015).
21. Sze, S. M. *Physics of Semiconductor Devices* (Wiley, 1981).
22. Jackson, W. B. Connection between the Meyer-Neldel relation and multiple-trapping transport. *Phys. Rev. B* **38**, 3595–3598 (1988).
23. Cullity, B. D. *Elements of X-Ray Diffraction* (Addison-Wesley, 1956).
24. Flewitt, A. J. *et al*. Stability of thin film transistors incorporating a zinc oxide or indium zinc oxide channel deposited by a high rate sputtering process. *Semicond. Sci. Technol.* **24**, 085002 (2009).

Acknowledgements

The support of this work by the Engineering and Physical Sciences Research Council (EPSRC) through project EP/M013650/1 is acknowledged.

Author Contributions

S.H. fabricated the samples and characterized them. S.H. and A.J.F. discussed the contents of the paper. Based on the discussion, S.H. did analysis using the proposed methods. S.H. and A.J.F. wrote the paper. All authors reviewed the manuscript.

Additional Information

Supplementary information accompanies this paper at doi:10.1038/s41598-017-05893-x

Competing Interests: The authors declare that they have no competing interests.

Publisher's note: Springer Nature remains neutral with regard to jurisdictional claims in published maps and institutional affiliations.